Determination of grain boundary geometry using TEM

Jang, H.; Farkas, D.; Hosson, J.T.M. De

Published in:
Journal of materials research

Publication date:
1992

Determination of grain boundary geometry using TEM

H. Jang[a] and D. Farkas
Department of Materials Engineering, Virginia Polytechnic Institute and State University, Blacksburg, Virginia 24061-0237

J. T. M. De Hosson
Department of Applied Physics, University of Groningen, Nijenborgh 18, 9747 AG, Groningen, The Netherlands

(Received 17 October 1991; accepted 19 March 1992)

An experimental method to obtain the grain boundary geometry using the transmission electron microscope is presented. The method allows Σ determination including grain boundary plane orientation. In order to determine the specialness of the grain boundary, three different criteria for maximum allowable deviations from exact CSL misorientations were examined. We tested these three criteria from a statistical distribution of grain boundary types in terms of Σ. We compared grain boundary distributions from other studies in Ni_3Al and found discrepancies among them. It seems that the discrepancy came from the different criteria for special boundaries in Σ determination and different experimental procedures they used. The statistical distribution of grain boundary plane orientations showed that low Σ boundaries ($\Sigma < 11$) were oriented to the plane of high density of coincident sites.

I. INTRODUCTION

It has long been known that the structure and energy of a grain boundary depend on the crystal misorientation between two adjacent grains and on the orientation of a particular interface plane adopted by the boundary. Several theoretical models have been proposed to describe the grain boundary structure.[1–10] Among the models, the coincident site lattice (CSL) representation of grain boundary structures has become dominant as a basis for grain boundary interpretation.[11,12] The CSL model is based on the degree of coincidence between lattice points from both grains across a boundary. The presence of coincident orientations can lead to properties that are different from other boundaries.[13] It is now generally accepted that grain boundaries can be "special" based on the degree of coincidence between two crystal points where the degree of coincidence can be calculated by the ratio between the volume of CSL lattice points and the volume of the basic lattice. The ratio has been symbolized by Σ. This approach mainly considered the macroscopic crystallography of the boundary without considering the detailed boundary structure after relaxation. Therefore, the variation of the grain boundary energy in this model is discontinuous with the misorientation of bicrystals. There exist two techniques to account for the discontinuity of the interfacial energy in the CSL model. One is the atomistic computer simulation of grain boundary structures, which gives the relaxed atomic structure in the grain boundary.[14,15] It is now well known that the detailed structure of grain boundaries has been studied successfully on various issues of grain boundary properties using atomistic computer simulations.[16–19] Another generalized model based on the CSL scheme was developed by Bollmann[6] to avoid the discontinuity with misorientation and to emphasize the periodic nature of the grain boundary structure.

Analysis of experimental data on the misorientation and grain boundary normal has not received as much attention as the theoretical boundary models. A recent review by Sutton and Balluffi,[20] after analyzing the available experimental results, suggested that the existing geometrical criteria for grain boundaries of low interfacial energy were not valid. They proposed that the variations of interfacial energy must be understood in terms of the atomic structure and details of the bonding at the interface. On the other hand, recent atomistic computer simulations showed that grain boundary planes with the high planar density of coincident sites (high Γ) have lower interfacial energies than low Γ planes.[21] The proposed criterion concerning Γ for the low interfacial energy has been supported by symmetry arguments.[21,22]

Furthermore, there is much evidence that the properties of special boundaries based on Σ and/or Γ may persist even for slight deviations from special misorientations.[23] Therefore, it is very important to define the criteria for allowable deviation from exact

[a]Current address: Department of Materials Science and Engineering, Technological Institute, Northwestern University, 2145 Sheridan Road, Evanston, Illinois 60208-3180.

CSL misorientations. A recent review on the criteria of specialness and allowable deviation from CSL orientation showed that there is no general criterion applicable to all the possible geometries of grain boundaries.[24]

In order to describe the grain boundary structure geometrically, nine geometric degrees of freedom need to be defined. Five degrees of freedom (macroscopic parameters) are related to the misorientation between two crystals and the other four degrees of freedom are associated with the translation of one crystal with respect to the other. The first five macroscopic parameters are the crystallographic parameters in terms of the CSL model and can be determined using transmission electron microscopy. The misorientation information requires three parameters for a rotation angle (θ) and a rotation axis ($h:l,k:l$) and two parameters for a grain boundary plane orientation ($p:r,q:r$). The other four degrees of freedom (microscopic parameters) are the rigid body translational state between two crystals: three parameters (t_1,t_2,t_3) for a rigid body translation of one crystal referred to the other and one parameter for the sequential periodicity (n) at the boundary plane, which is possible to determine using high resolution electron microscopy[25] or atom probe field ion microscopy.[26] However, these four microscopic parameters are not usually considered in the CSL model.

There have been numerous reports about statistical distribution of misorientation angles and specifically Σ distributions. However, in the literature, there are no studies of statistical distribution of grain boundary plane orientations and the relation to Σ. We explore this question in the present work.

Two different techniques have been used for the determination of rotation axis/angle pairs to determine the Σ value based on the CSL model. Young *et al.*[27] characterized the misorientation information as a 3×3 matrix whose columns represent the direction cosines of crystal 1 with respect to crystal 2 using Kikuchi patterns from each grain. The procedure involved the selection of three orthogonal coordinate systems, such as a crystal frame, a pattern frame, and a reference frame, to obtain the misorientation information of bicrystals. Another approach is based on standard stereographic procedures.[28,29] Using two or three pairs of diffraction patterns, this method is based on the fact that the pattern zone axes in both grains should be parallel and that the axis of misorientation lies on a zone which is equidistant from the pattern zone. This zone is, then, represented on the stereogram as a great circle which bisects the great circle through the two or three pattern zones. The first method, however, has several sources of error: particularly in the establishment of the reference frame and in obtaining the effective camera length. The second method also involves an unavoidable inaccuracy in plotting the poles and in manipulating the stereogram.

Determination of a grain boundary plane normal is based mainly on the crystallographic analysis concerning the geometry of the boundary plane. When the grain boundary plane is oriented parallel to the beam axis, the determination of grain boundary normal is straightforward. However, when the grain boundary plane is highly inclined, the error from the inaccuracy in the atomic scattering factor is introduced in determining the thickness of a foil and, consequently, the grain boundary normal obtained through standard procedures seems unreliable. Recently, it became known that the convergent beam technique could reduce the error in determining the thickness of the sample to around $\pm 2\%$.[30] Then, the geometrical analysis of grain boundary plane orientation using the foil thickness became a solid technique to obtain the accurate grain boundary plane normal.

In the present work, a schematic way of determining the grain boundary geometry is presented, which gives misorientation information with the grain boundary plane normal. The method of determining the misorientation information in terms of Σ is basically the same as the analytical method,[27] but the complexity of constructing three different frames is avoided by tilting the specimen. Three different methods to obtain the grain boundary plane normal are presented, depending on the grain boundary plane orientations. Using this method, statistical distributions of grain boundary types of Ni_3Al were obtained and the influence of criteria for the maximum allowable deviations from exact CSL orientation is discussed. The statistical distribution is compared with previously published distributions of Σ values in Ni_3Al. Finally, the statistical distribution of grain boundary normals was obtained to investigate the occurrence of high Γ planes in polycrystalline Ni_3Al.

II. DETERMINATION OF THE GRAIN BOUNDARY GEOMETRY

The whole procedure of determining the grain boundary geometry starts with precise orientation information of single crystals. Then, using the orientation information from both crystals, the relative misorientation of a bicrystal (rotation axis and angle) can be determined by constructing a matrix. As a final step, the orientation of grain boundary planes will be determined by trace analysis.

A. Precise orientation determination of single crystal orientation

The determination of a crystal orientation can be done very accurately if convergent beam electron diffraction (CBED) techniques are available. The electron beam direction with respect to a crystal can be determined

within the error range of 0.05° using CBED. The angle of convergence must be large enough to obtain a large field of view. In the CBED pattern Kikuchi lines are much clearer as compared to normal selected area diffraction patterns (SAD). This is primarily caused by the fact that the sampled volume in CBED is much smaller than in SAD.[31] Accordingly, the contrast of the Kikuchi lines is less smeared out by strain, bending of the crystal, or defects. Secondly, elastically scattered electrons also contribute to the Kikuchi lines, since the angle of convergence is larger than the Bragg angle of many planes parallel to the incident beam direction.

Application of the CBED technique to determine the precise orientation of a crystal can be done using the three pole solution. The three pole solution requires three pairs of non-parallel Kikuchi lines to obtain an incident beam direction, B, unambiguously from a pattern.[32] Three such pairs are shown in Fig. 1(a). The dashed lines are the traces of the intersection of $\{hkl\}$ planes in the Ewald sphere. Therefore, points A, B, and C in Fig. 1(b) correspond to the zone axis of the intersection in the reflecting planes.

In order to index Kikuchi lines, the spacing of each Kikuchi pair has to be determined. If the crystal is cubic, then, the spacing of each Kikuchi line (D) is inversely proportional to the d-spacing of the particular ($h\,k\,l$) plane (d), and $D_1d_1 = \lambda L, D_2d_2 = \lambda L, D_3d_3 = \lambda L$ where λ is the wavelength of the electron for a certain acceleration voltage of the TEM and L is the effective camera length. From the measured spacings of D_1, D_2, D_3 and their ratios, the tentative indices of Kikuchi lines can be assigned from the table of d-spacings. The correctness of the index assignment can be checked by measuring the angles ϕ_1 ϕ_2 ϕ_3, which are the angles between two non-parallel Kikuchi lines, and comparing with calculated values.

The procedure described above is, however, quite slow and particularly inappropriate for a large number of boundaries. Particularly, the procedure of consulting the tables of d-spacings to find a tentative value of ($h\,k\,l$) is extremely tedious for high index Kikuchi lines for the ordered structure because of superlattice Kikuchi lines. In order to overcome the difficulty of finding pole indices, a montaged Kikuchi map or a computer generated Kikuchi map can be used as an alternative method. For cubic crystals a complete map can be obtained within the triangle defined by [001], [011], and [111] poles. Once the Kikuchi map is constructed, a Kikuchi pattern from a single crystal can easily be indexed by comparing with the map.

When the three poles are indexed, the beam direction, B, can be obtained analytically. With the indices of three poles, $[p_1q_1r_1]$, $[p_2q_2r_2]$, $[p_3q_3r_3]$, the beam direction $[uvw]$ can be determined by solving three simultaneous equations[33]:

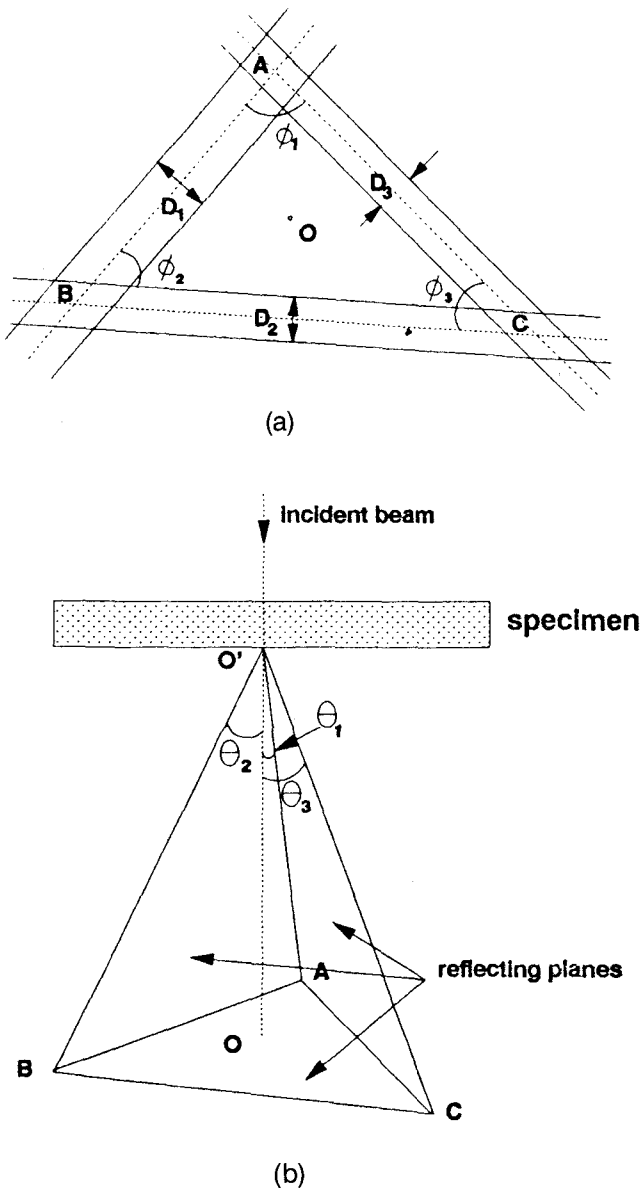

FIG. 1. (a) Three pairs of Kikuchi lines for the three pole solution; dotted lines are projections of reflecting planes intersected at A, B, and C. (b) Projection of the responsible reflecting planes relative to the specimen.

$$\cos\theta_1 = \frac{up_1 + vq_1 + wr_1}{\sqrt{u_2 + v_2 + w_2}\,\sqrt{p_1^2 + q_1^2 + r_1^2}} \tag{1}$$

$$\cos\theta_2 = \frac{up_2 + vq_2 + wr_2}{\sqrt{u_2 + v_2 + w_2}\,\sqrt{p_2^2 + q_2^2 + r_2^2}} \tag{2}$$

$$\cos\theta_3 = \frac{up_3 + vq_3 + wr_3}{\sqrt{u_2 + v_2 + w_2}\,\sqrt{p_3^2 + q_3^2 + r_3^2}} \tag{3}$$

The angles θ_1, θ_2, θ_3 are the angles OO′A, OO′B, OO′C in Fig. 1(b). These angles can be calculated by employing the average calibration factor K rather than

calculating from the effective camera length which may involve errors.

$$K_1 = \frac{\text{angle(AO'B)}}{D_{\overline{AB}}}, K_2 = \frac{\text{angle(BO'C)}}{D_{\overline{BC}}}, K_3 = \frac{\text{angle(CO'A)}}{D_{\overline{CA}}} \quad (4)$$

$$K_{\text{average}} = \frac{K_1 + K_2 + K_3}{3} \quad (5)$$

$$\theta_1 = K_{\text{average}} \cdot D_{\overline{AO}} \quad (6)$$

$$\theta_2 = K_{\text{average}} \cdot D_{\overline{AO}} \quad (7)$$

$$\theta_3 = K_{\text{average}} \cdot D_{\overline{AO}} \quad (8)$$

As a summary, the procedure to obtain the single crystal orientation from Kikuchi patterns is as follows: (i) Index three poles using the Kikuchi map or using the table of *d*-spacings. (ii) Measure the distances $\overline{AB}$, $\overline{BC}$, $\overline{CA}$, $\overline{AO}$, $\overline{BO}$, $\overline{CO}$. (iii) Calculate the calibration factor, K, from (ii). (iv) Calculate the angle θ_1, θ_2, θ_3 using average calibration factor, K_{average}. (v) Solve three simultaneous Eqs. (6), (7), and (8) to obtain the indices of the incident beam axis [*uvw*].

B. Determination of the grain boundary misorientation

A brief description of the procedure for obtaining grain boundary misorientation information is now presented. In general, the grain boundary misorientation can be expressed in terms of the rotation axis and angle which can be derived from a rotation matrix. The rotation matrix (3 × 3) characterizes the misorientation between two crystals, and columns of the matrix represent the direction cosines of grain 1 to grain 2.[34] In order to obtain the rotation matrix experimentally, two pairs of Kikuchi patterns are used. The procedure to obtain the rotation matrix is as follows:

(i) Construct a simple matrix formulation from the crystal orientation information:

$$[M]_{\text{II}}[R] = [M]_{\text{I}} \quad (9)$$

where $[R]$ is a rotation matrix corresponding to the misorientation between two crystals and $[M]_{\text{I}}$, $[M]_{\text{II}}$ are matrices according to each grain. Each row in matrices $[M]_{\text{I}}$, $[M]_{\text{II}}$ represents the single crystal orientation from each grain before tilt and after tilt. By rearranging Eq. (9):

$$[R] = [M]_{\text{I}}[M]_{\text{II}}^{-1} \quad (10)$$

where the full formation of the rotation matrix can be described as follows:

$$\begin{pmatrix} a_{11} & a_{21} & a_{31} \\ a_{12} & a_{22} & a_{32} \\ a_{31} & a_{23} & a_{33} \end{pmatrix} = \begin{pmatrix} h_1 & k_1 & l_1 \\ h_2 & k_2 & l_2 \\ h_3 & k_3 & l_3 \end{pmatrix}_{\text{I}} \times \begin{pmatrix} h_1 & k_1 & l_1 \\ h_2 & k_2 & l_2 \\ h_3 & k_3 & l_3 \end{pmatrix}_{\text{II}}^{-1} \quad (11)$$

where the column vectors of the rotation matrix $[R]$ represent the direction cosines between the Cartesian axes from both grains across a boundary.

(ii) Calculate the rotation angle from the equation below[35]:

$$\theta = \text{acos}\left(\frac{a_{11} + a_{22} + a_{33} - 1}{2}\right) \quad (12)$$

(iii) Calculate the rotation axis [*HKL*] from the following equation[35] except for the case of the 180° rotation angle:

$$H = a_{32} - a_{23}$$
$$K = a_{13} - a_{31}$$
$$L = a_{21} - a_{12} \quad (13)$$

When the rotation angle is 180°, the formulation above will give a rotation axis as [000], which does not have any physical meaning. From the general form of the rotation matrix, the rotation axis in the case of the 180° rotation angle can be obtained from the following equations:

$$H:K:L = (a_{11} + 1):a_{12}:a_{13} \quad (14)$$

If [*HKL*] from Eq. (14) is [000], then:

$$H:K:L = a_{21}:(a_{22} + 1):a_{23} \quad (15)$$

If [*HKL*] from Eq. (15) is [000], then:

$$H:K:L = a_{31}:a_{32}:(a_{33} + 1) \quad (16)$$

The relative orientation of two cubic crystals can be described in 24 different ways, since a right-handed orthogonal coordinate system with axes ⟨100⟩ type directions of a cubic lattice can be chosen in 24 different ways corresponding to the symmetry operation of the point group 4 3 2.[35] Tables that list 24 equivalent rotation axes/angles with a rotation matrix for each Σ are available in the literature.[12,35] The tables are essential in order to determine the Σ from the experimentally obtained rotation matrix. In particular, tables in the order of Σ and in the order of the rotation angle prepared by us were of great help.[47] A search for a Σ begins with either the lowest or 180° rotation angle by comparing the rotation axis from experimental and theoretical values. However, the search with lowest angle was preferred since the angle variation near 180° is not sensitive to cosine values in Eq. (12).

C. Determination of the grain boundary plane orientation

The grain boundary plane normal can be determined in several different ways, depending on the inclination of boundary planes. The simplest situation is the case when the grain boundary plane can be oriented edge-on both before and after tilt. Then the grain boundary plane normal can be directly calculated by the cross product of two crystal orientations from the same grain. Although this procedure is simple, it is not possible to apply this method to highly inclined grain boundary planes because of the limitation in the specimen tilting device. Secondly, the grain boundary normal can be obtained using dislocation line directions that are contained in the boundary plane and the direction of the grain boundary trace at the foil surface.[37] In order to determine a dislocation line direction, at least three different beam directions with slight tilts are needed.

The more general way of determining the grain boundary plane normal is the conventional trace analysis. The first step in this technique is to determine the thickness of the sample, which can be done by counting fringes from grain boundary planes or using a convergent beam technique. The foil thickness measurement using the fringe counting method has an accuracy of $\pm 10\%$ due to the inaccuracy in determining the atomic scattering amplitude.[37] On the other hand, the technique using CBED enables us to determine the specimen thickness with an accuracy around $\pm 2\%$.[38]

After the specimen thickness is determined, the next step is to ascertain the top foil surface in the micrograph, which depends on the inclination of a grain boundary plane. The easiest way to determine the grain boundary traces at the top foil surface is by remembering that the nature of the first and last fringes in the bright-field image are different, while those of the dark-field image are the same.[39] Finally, the grain boundary plane normal can be determined by considering directions of grain boundary traces and the foil surface using trace analysis, foil thickness, and width of projected grain boundary plane, followed by an angle between surface and grain boundary plane to obtain the direction.

III. CRITERIA FOR DEVIATIONS FROM CSL MISORIENTATIONS

The CSL theory would be of very limited applicability if the special structure occurred only at exact CSL misorientations. In fact, there is much evidence that the special properties may persist for deviations from special misorientations.[23,40] It was first suggested by Read and Shockley[41] that when there is such a deviation, a low energy interface may be maintained by an array of dislocations similar to those in a low angle grain boundary. The effect of the dislocation network is to condense the mismatch onto lines of misfit. In terms of the structural unit model,[42] it can be understood as the superimposition of a dislocation array on a CSL grain boundary, which is equivalent to adding periodically a unit characteristic of a different CSL. As the deviation increases, the spacing between dislocations decreases. Eventually, the cores overlap and the dislocations lose their identities. The criterion for deviation from CSL misorientations is discussed in this section and consideration will be given to the calculation of the actual deviation of experimentally obtained grain boundary orientations from exact CSL orientations and the allowable maximum deviation at which such dislocations exist.

A. Deviations from CSL orientations

The method to estimate deviation from the CSL misorientation for the bicrystal whose misorientation is close to a CSL relationship has been controversial. There are two methods that are generally used: a method by Kokawa *et al.*[43] and an analytical approach by Bleris *et al.*[36] Kokawa *et al.* calculated the deviation angle as a function of two components, the deviation of a rotation angle and the deviation of a rotation axis. On the other hand, the analytical method by Bleris *et al.*[36] compared the rotation matrix obtained from the experiment with the matrix from the exact CSL. The latter analytical method correctly results in the same value of deviation from the 24 equivalent axis/angle expressions. However, the method by Kokawa *et al.* generates different deviations from each axis/angle expression in 24 equivalent expressions. Therefore the analytical method by Bleris *et al.*[36] should be used to determine the actual deviation unambiguously from the exact CSL orientation. The analytical method uses matrices from the experiment and the exact CSL. Let's assume M_e, an actual rotation matrix from a real bicrystal, and M_{CSL} as a CSL misorientation matrix. According to the standard procedure of the matrix calculation, the matrix that expresses the deviation is $M_d = M_e(M_{\mathrm{CSL}})^{-1}$, where $(M_{\mathrm{CSL}})^{-1}$ is the inverse of M_{CSL}. Then the deviation angle $\Delta\theta_d$ is deduced from the trace of M_d:

$$\Delta\theta_d = \mathrm{acos}\left(\frac{M_{11} + M_{22} + M_{33} - 1}{2}\right) \qquad (17)$$

B. The maximum allowable deviation (criteria for specialness)

Considerable experimental evidence has shown that special boundaries maintain their properties of low energy interfacial structures when the boundary deviates slightly from the exact CSL misorientation. Several criteria were suggested for the maximum allowable deviation at which the boundary sustained its special properties.

According to Read and Shockley,[41] the maximum deviation of a boundary from a special misorientation is given by

$$\Delta\theta_c = \frac{\mathbf{b}}{d_{\min}} \tag{18}$$

where **b** is the average Burgers vector in the DSC lattice and $d_{\min}$ is the closest allowed spacing of the dislocations which is of the order of the boundary periodicity p. It is not easy to give a general expression for $\Delta\theta_c$ as a function of Σ. However, in general, boundary periodicity, p, varies with the boundary plane and the Burgers vector depends on the grain boundary plane orientations. Warrington and Grimmer[44] proposed that the mean value of p varies as a function of $\Sigma^{1/3}$ and the mean value of b varies as a function of $\Sigma^{-1/3}$ since the volume of the CSL unit cell varies as a function of Σ and the volume of the unit cell of the Burgers vectors varies as a function of Σ^{-1}. Then the maximum allowable deviation angle from exact CSL misorientations is

$$\Delta\theta_c = \theta_0\Sigma^{-2/3} \tag{19}$$

where θ_0 is constant for all CSLs and is the maximum deviation angle for low angle grain boundaries. Considering the special case of DSC Burgers vectors lying in a boundary plane perpendicular to a ⟨100⟩ misorientation axis, p varies as $\Sigma^{1/2}$ and b varies as $\Sigma^{-1/2}$. Then the maximum deviation is[45]

$$\Delta\theta_c = \theta_0\Sigma^{-1} \tag{20}$$

On the other hand, Brandon's criterion[5] which has been used by many researchers considered the boundary periodicity only in the special case of boundary plane perpendicular to a ⟨100⟩ misorientation axis. The Brandon criterion is

$$\Delta\theta_c = \theta_0\Sigma^{-1/2} \tag{21}$$

Therefore, the criterion can be adjusted to specific grain boundaries, depending on the geometry of the grain boundary, as considered by Ishida and Mclean[45] for ⟨100⟩ twist grain boundaries or based on the periodicity of the grain boundary plane, as considered by Brandon[5]; there seems to be no criterion that is applicable to all cases of grain boundary geometries. The choice of a criterion can influence the statistical distribution of Σ in a polycrystal. The effects of choosing different criteria will be discussed later.

The estimation of the maximum deviation angle for low angle grain boundaries, θ_0, is another factor to be considered in determining the maximum tolerable deviation angle from exact CSL misorientation. First, Read and Shockley[41] suggested that a valid limit of θ_0 is 15° from their dislocation model of the grain boundary structure. On the other hand, TEM observation of the maximum deviation angle of observable discrete grain boundary dislocations showed, by using a conventional TEM technique in a two beam dynamical condition, that the maximum allowable deviation angle of the low angle boundary was 8°. However, the discrete image of the grain boundary dislocations in the figure will be smeared at the higher value of deviation angle due to the overlap of strain fields from the adjacent dislocations, and it won't be able to measure the distance between grain boundary dislocations.[24] Recently, Ichinose and Ishida[46] showed evidence of maintaining discrete dislocations up to 15°, using high resolution electron microscopy.

The choice of a criterion for the maximum deviation, $\Delta\theta_c$, can definitely influence the statistical distribution of the grain boundary types of the material. The maximum deviation angles according to the different criteria are listed for low Σ's in Table I.

IV. EXPERIMENTS

The effects of grain boundary type distributions using different criteria were investigated. Moreover, the statistical distribution of the grain boundary plane normal was also studied to obtain the transition point of the Σ value for a random boundary. The material investigated was ordered Ni_3Al with the chemical composition of 24 at. % Al/76 at. % Ni with 500 ppm B. The samples were vacuum annealed at 1050° for 6 h to reduce the defect density and control the average grain size of the material. The average grain size of the material after annealing was about 5.4 μm in diameter. A final thinning procedure was done by a twin-jet electrochemical polisher with the chemical solution of 70 vol. % CH_3OH + 30 vol. % HNO_3. Experimental work was carried out using a JEOL 200CX transmission electron microscope.[47]

TABLE I. Maximum deviation angle according to three different criteria for $\Delta\theta_c$.

Criteria	$\Sigma = 1$	$\Sigma = 3$	$\Sigma = 5$	$\Sigma = 7$	$\Sigma = 9$	$\Sigma = 11$	$\Sigma = 13$	$\Sigma = 15$	$\Sigma = 17$	$\Sigma = 19$
$\Delta\theta_c = 8\Sigma^{-1}$	8	2.67	1.60	1.14	0.89	0.73	0.62	0.53	0.47	0.42
$\Delta\theta_c = 15\Sigma^{-2/3}$	15	7.21	5.13	4.10	3.47	3.03	2.71	2.47	2.27	2.11
$\Delta\theta_c = 15\Sigma^{-1/2}$	15	8.66	6.71	5.67	5.00	4.52	4.16	3.87	3.64	3.44

TABLE II. The Σ distribution of grain boundaries, expressed as percentages, from polycrystalline Ni_3Al (24% Al with 500 ppm boron) according to three different criteria.

Criteria\Σ	3	5	7	9	11	13	17	19	21	25	27	29	>29
Brandon[5]	15.1	1.4	2.7	1.4	4.1	1.4	1.4	1.4	1.4	1.4	1.4	1.4	66.5
Warrington *et al.*[44]	15.1	1.4	2.7	1.4	2.7	1.4	0	1.4	1.4	0	0	0	72.5
Ishida *et al.*[45]	15.1	1.4	1.4	0	1.4	0	0	0	0	0	0	0	80.7

A. Statistical distribution of Σ values

From the geometrical analysis of grain boundaries using TEM, a statistical distribution of grain boundary types was obtained from polycrystalline Ni_3Al. Grain boundary misorientations were measured from 73 boundaries. In order to determine the proportion of special boundaries from randomly oriented polycrystals, three different criteria for maximum deviation were examined. Table II shows the results of choosing different criteria in the statistical distribution of grain boundary types. As expected from Table I, frequencies increase as Σ increases. Table III shows a summary of the measurements of the present work and results from other researchers about Σ distributions in ductile and brittle Ni_3Al. In these data we observe wide variations in the amounts of $\Sigma = 3$ and low angle boundaries (LAB). This is probably due to the different methods of collecting the grain boundaries and the thermal history of the sample. Additional differences in the percentage of random and low Σ boundaries can be related to the criterion used for acceptable deviations from exact CSL misorientations. In addition, some investigators consider low Σ for $\Sigma = 5$–19 and others take $\Sigma = 5$–29 or $\Sigma = 5$–49. If the latter criteria are used, some differences between ductile and brittle material can be identified. These differences are not significant if $\Sigma > 19$ are taken as random.

B. Statistical distribution of grain boundary planes

The grain boundary energy of a certain Σ grain boundary varies as a function of the boundary plane orientation. Thus grain boundary plane orientations also should be considered besides the value of Σ. This has been suggested by grain boundary energy calculations using atomistic simulation.[21] A review of symmetry arguments for low interfacial energy proposed that the energetically stable grain boundary structure can be related to the high planar density of coincident sites.[21,22] The planar CSL site density depends on both Σ and the grain boundary plane orientation. Therefore, the statistical distribution of the grain boundary plane normal is important in the investigation of the energetically stable orientation of grain boundary planes and the role of Σ in the grain boundary properties. In addition, this statistical distribution will help identify a threshold value of Σ as a random boundary regardless of the lattice coincidence between two grains.

Using the methods in Sec. II.C, the statistical distribution of grain boundary plane orientations was obtained up to $\Sigma = 29$ from 73 grain boundaries. Σ was determined employing traditional Brandon's criteria.[4,5] Figure 2 shows the result on grain boundary plane orientations adopted in each Σ in Ni_3Al. In the case of $\Sigma = 3$ grain boundaries (twin boundaries), all planes showed {111} or {112} plane orientation. These orientations are the lowest energy, {111}, and second lowest energy,

TABLE III. Comparison of Σ distributions obtained for Ni_3Al, Ni, and Al in %.

Material	Low angle	$\Sigma = 3$	$\Sigma = 5$–29	Random
Cast Ni_3Al[a]	8.7	0	5.8	85.5
Recrystallized Ni_3Al, grain size: 0.3 mm[a]	8.1	12.4	4.4	75.1
Recrystallized Ni_3Al, grain size: 1 mm[a]	3.0	14.5	3.0	79.5
B doped Ni_3Al 24.8% Al[b]	0	15.1	19.4	65.5
B doped Ni_3Al 24.8% Al, grain size: 0.06 mm[c]	26.0	0	25.0	49.0
B doped Ni_3Al 24.8% Al, grain size: 0.16 mm[c]	26.0	0	23.0	51.0
B doped Ni_3Al 25% Al, grain size: 0.15 mm[c]	17.0	4.5	11.5	67.0
B doped Ni_3Al 25% Al, grain size: 0.28 mm[c]	18.0	5.0	12.0	65.0
Annealed pure Ni_3Al[d]	2.2	25.1	3.8	68.9
Annealed B doped Ni_3Al[d]	1.8	20.1	5.3	72.8
Ni_3Al[e]	3.3	...	15.9	80.8

[a]Hanada *et al.*[54]
[b]Present work
[c]Farkas *et al.*[23]
[d]Mackenzie *et al.*[55] These authors considered grain boundaries as random boundaries when $\Sigma > 19$.
[e]Lin and Pope.[15] These authors considered low Σ boundaries when $\Sigma = 3$–49.

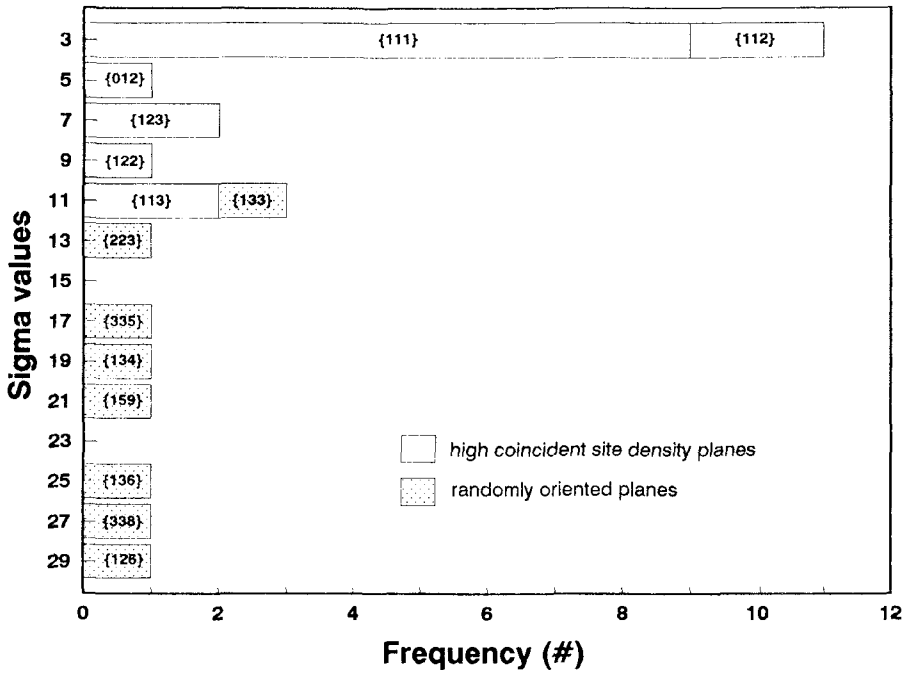

FIG. 2. Distribution of grain boundary plane orientation up to $\Sigma = 29$.

{112}, configurations for $\Sigma = 3$ grain boundaries. The low energy configuration of the grain boundary is expected to have plane indices (*hkl*) which follow a rule of $n\Sigma = h^2 + k^2 + l^2$, where n is 1 or 2, since these are the planes of high coincident site density. From the investigation of 73 grain boundary plane normals, we found that the trend of having a high coincident site density plane was maintained on low Σ boundaries up to $\Sigma = 9$, and random orientations of grain boundary planes became dominant after $\Sigma = 11$. The trend of deviating from the energetically stable geometries after $\Sigma = 11$ is believed to come from the fact that the driving force to choose energetically stable orientations of boundary planes during material processing is not strong in high Σ boundaries. The occurrence of particular grain boundary planes for a given misorientation is expected from the symmetry of the coincidence lattice. Given the energetic driving forces for the choice of particular grain boundary planes for given misorientation, one correspondingly expects to observe grain boundary steps. Figure 3 shows an example of $\Sigma = 3$ where the grain boundary is clearly oriented along very particular planes. In this case there is a clear energetic advantage for the grain boundary to be located in {111} planes. For a higher value of Σ the driving force is probably lower, and this type of phenomenon was not widely observed.

V. DISCUSSION

A large amount of theoretical and experimental studies on the grain boundary structure has been reported during the past several decades. The main thrust of the grain boundary studies has been focused on the possible relationship between the grain boundary structure and its properties such as grain boundary strength, creep, corrosion behavior, etc., so that it is now generally accepted that grain boundaries with low interfacial energy play a major role in the grain boundary properties and behavior. Recently, new materials such as high temperature intermetallic compounds show that grain boundaries may be a controlling factor in the mechanical properties of the material.[48–50] In particular, the breakthrough of ductilizing an intermetallic compound Ni_3Al triggered various investigations on grain boundary structures that

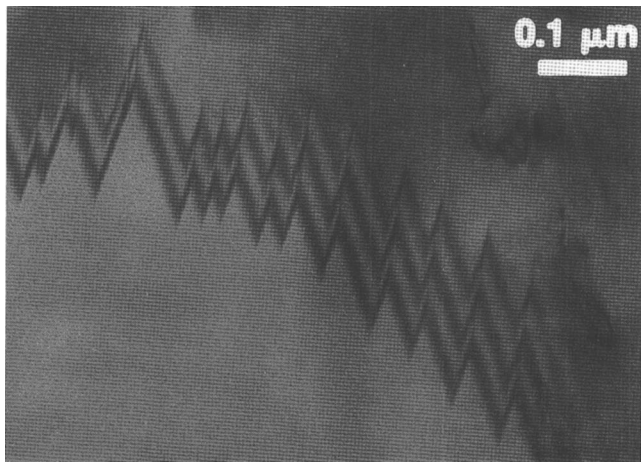

FIG. 3. A micrograph of a $\Sigma = 3$ grain boundary with {111} faceted planes.

would maintain the superior properties of intermetallics but reduce the inherent grain boundary brittleness.[51]

Much research has been done on the relationship between Σ distribution of grain boundaries and the ductile-brittle behavior of materials. However, there have been discrepancies in the results.[52–57] These may come from experimental methods to obtain the grain boundary geometry and the criteria for the specialness of the grain boundary or from the differences in material processing. The main purpose of the present work was, therefore, to present experimental techniques that obtain accurate grain boundary geometries using TEM and to compare the existing criteria for the specialness of grain boundaries based on the CSL models with experimentally obtained grain boundary type distributions. Also, in most studies, the orientation of the grain boundary plane is not determined. Boundaries with the same Σ but different grain boundary plane orientation may behave in a different way. However, in most studies about statistical distribution of grain boundary types, the grain boundary plane orientation was underestimated and was not considered experimentally. In the present work we have tried to analyze possible favored locations for the grain boundary plane for a given Σ.

There have been many studies on a practical approach for the determination of the crystallography of grain boundaries using TEM.[27–29,58,59] Most of the methods were based on the CSL model of the grain boundary, giving attention to determination of the rotation angle and axis followed by grain boundary types in terms of Σ, without considering the grain boundary normal. Moreover, the accuracy of methods of determining the grain boundary geometry using TEM has remained in doubt. The procedure presented in this work encompasses all the elements that specify the grain boundary geometries in terms of the CSL model, including grain boundary misorientation axis/angle and grain boundary plane normals, with high accuracy.

The criteria about the allowable deviation from exact CSL misorientations were examined. The criterion proposed by Brandon[5] has been developed in the special case of boundary plane perpendicular to a $\langle 100 \rangle$ misorientation axis by considering the boundary periodicity only. Consequently, Brandon's criterion is inapplicable for the investigation of grain boundary distribution from randomly oriented polycrystals, although many researchers have employed the criterion for the maximum allowable deviation from the exact CSL misorientation. Instead, the criterion proposed by Warrington and Grimmer[44] seems appropriate for the statistical investigation of the grain boundary distribution from polycrystals, i.e., the mean value of boundary periodicity and DSC Burgers vector in terms of reciprocal volume density of coincident sites. For the estimation of the maximum deviation angle for low angle boundaries, high resolution electron microscopy showed the same value of 15° for θ_c, which was suggested by Read and Shockley.[41] Consequently, the criterion by Warrington and Grimmer[44] with $\theta_0 = 15°$ was used in our study for the statistical distribution of grain boundary types collected from randomly oriented polycrystalline materials.

In our study of the distribution of grain boundary plane orientation, boundary normals were oriented to the plane of high density of coincident sites for low Σ boundaries up to $\Sigma = 9$. This result implies that most of the grain boundary plane with low Σ values would be oriented in high Γ planes since the driving force for energetically stable geometries of grain boundaries is high. However, the driving force for high Σ boundaries is small during the thermal processing of polycrystals such as solidification, recrystallization, or grain growth and the grain boundary plane remains as low Γ planes. Our work suggests the value $\Sigma = 11$ as a cutoff for the grain boundary plane orientation along a favored plane in the CSL. This cutoff value is possibly dependent on the details of materials processing and should not be taken for general validity. We believe that the grain boundary plane orientation is an extremely important parameter in determining the grain boundary behavior. It will, therefore, be very interesting to test the validity of the cutoff value suggested here for different processing conditions and in different materials. Particularly, it will be very interesting to test if this cutoff changes upon microalloying Ni_3Al with boron. There have been several studies on the statistical distribution of grain boundary types in terms of Σ only from polycrystals.[52–57] They considered grain boundaries with relatively high Σ boundaries as random boundaries after $\Sigma = 29$ or $\Sigma = 49$ without detailed investigation of grain boundary plane orientations. On the other hand, our investigation of grain boundary plane orientation showed that the threshold value for random boundaries is around $\Sigma = 11$, which is considerably lower than 29 or 49. However, as mentioned above, the statistical distribution of grain boundary types is sensitive to the thermal[60] and mechanical[61,62] histories of the sample, and one should be very careful in drawing conclusions from the statistical distribution of grain boundary types as to speculating on possible relationships with mechanical properties.

VI. CONCLUSIONS

A method to determine the grain boundary geometry, including a rotation axis, a rotation angle, and grain boundary plane normal, was presented. By tilting the specimen, a rotation matrix was constructed to obtain misorientation information between two grains. In comparison to other methods, the method presented here was easy to do with high precision. Methods of determining

the grain boundary normal were also illustrated according to different boundary plane geometries. The CBED technique was introduced to determine the specimen thickness which is necessary in the trace analysis to obtain the grain boundary plane normal.

A statistical distribution of grain boundary types of Ni_3Al was obtained according to three different criteria for the maximum allowable deviation from the exact CSL misorientation. The result showed that the choice of the criteria changed the Σ distribution of the material. There seemed no criterion applicable to all the possible geometries of grain boundaries. Among the criteria, however, criterion by Warrington and Grimmer[44] seemed more appropriate than others for randomly oriented polycrystalline materials. There were many discrepancies in the statistical distributions of Ni_3Al among the various results from different sources. From the statistical investigation of grain boundary normals, the trend of having high coincident site density planes was maintained up to $\Sigma = 9$ and grain boundary planes after $\Sigma = 11$ were oriented randomly regardless of Σ values.

ACKNOWLEDGMENTS

This work was partly supported by the Department of Energy, Energy Conversion and Utilization Technologies (ECUT) program under Subcontract No. 19X-89768V with Martin Marietta Energy Systems Inc. and was monitored by Oak Ridge National Laboratories.

REFERENCES

1. D. McLean, *Grain Boundaries in Metals* (Clarendon Press, Oxford, 1957).
2. J.C.M. Li, J. Appl. Phys. **32**, 525 (1961).
3. K.T. Aust, in *Recovery and Recrystallization of Metals,* edited by L. Himmel (Interscience Publishers, New York, 1962), p. 131.
4. D.G. Brandon, B. Ralph, S. Ranganathan, and M.S. Wald, Acta Metall. **12**, 813 (1964).
5. D.G. Brandon, Acta Metall. **14**, 1479 (1966).
6. W. Bollmann, *Crystal Defects and Crystalline Interfaces* (Springer-Verlag, Berlin, 1970).
7. W. Bollmann, J. Microsc. **102**, 233 (1974).
8. H. Gleiter, Phys. Status Solidi (b) **45**, 9 (1971).
9. P.H. Pumphrey, Scripta Metall. **6**, 107 (1972).
10. B. Ralph, J. de Physique **C4**, No. 1036, C4-71 (1975).
11. A. Brokman and R.W. Balluffi, Acta Metall. **29**, 1703 (1981).
12. H. Grimmer, W. Bollmann, and D.H. Warrington, Acta Cryst. **A30**, 197 (1974).
13. D.H. Warrington, *Grain Boundary Structure and Kinetics,* ASM Seminar (1980), p. 1.
14. R.C. Pond and V. Vitek, Proc. R. Soc. Lond. B **357**, 453 (1977).
15. R.C. Pond, Proc. R. Soc. Lond. B **357**, 471 (1977).
16. S.M. Foiles and M.S. Daw, J. Mater. Res. **2**, 5 (1987).
17. S.P. Chen, D.J. Srolovitz, and A.F. Voter, J. Mater. Res. **4**, 62 (1989).
18. J. Th. M. De Hosson, B.J. Pestman, F.W. Schapink, and F.D. Tichelaar, in *Interfacial Structure, Properties, and Design,* edited by M.H. Yoo, W.A.T. Clark, and C.L. Briant (Mater. Res. Soc. Symp. Proc. **122**, Pittsburgh, PA, 1988), p. 145.
19. D. Farkas and H. Jang, Phys. Rev. B, No. 16, 11 769 (1989).
20. A.P. Sutton and R.W. Balluffi, Acta Metall. **35**, No. 9, 2177 (1987).
21. D. Farkas, in *High Temperature Ordered Intermetallic Alloys III,* edited by C.T. Liu, A.I. Taub, N.S. Stoloff, and C.C. Koch (Mater. Res. Soc. Symp. Proc. **133**, Pittsburgh, PA, 1989), p. 137.
22. R. Wyckoff, The Analytical Expression of the Results of the Theory of Space Groups (Carnegie Institution, Washington, DC, 1930).
23. H. Gleiter and B. Chalmers, Prog. Mater. Sci. (B), 16 (1972).
24. M. Dechamps, F. Baribier, and A. Marrouche, Acta Metall. **35**, No. 1, 101 (1987).
25. K.L. Merkle, Colloque De Physique C1, **51**, C1-251 (1990).
26. D.N. Seidman, in *Characterization of the Structure and Chemistry of Defects in Materials,* edited by B.C. Larson, M. Rühle, and D.N. Seidman (Mater. Res. Soc. Symp. Proc. **138**, Pittsburgh, PA, 1989), p. 315.
27. C.T. Young, J.H. Steeles, and J.L. Lytton, Metall. Trans. **4**, 2081 (1973).
28. C. Goux, Bull. cercle Etudes Metaux **8**, 185 (1961).
29. V. Randal and B. Ralph, J. Mater. Sci. **21**, 3823 (1986).
30. P.M. Kelly, A. Jostons, R.G. Blake, and J.G. Napier, Phys. Status Solidi (a) **31**, 771 (1975).
31. N.J. Long, M.H. Loretto, and R.E. Smallman, *Proc. 7th European Congress on Electron Microscopy* **1**, 152 (1980).
32. M. von Heimendahl, W. Bell, and G. Thomas, J. Appl. Phys. **35**, 3614 (1964).
33. G. Thomas and M.J. Goringe, *Transmission Electron Microscopy of Materials* (John Wiley & Sons, New York, 1979).
34. F.F. Lange, Acta Metall. **15**, 311 (1967).
35. D.H. Warrington and P. Bufalini, Scripta Metall. **5**, 771 (1971).
36. G.L. Bleris, J.G. Antonopoulous, T.H. Karakatos, and P. Delvavignette, Phys. Status Solidi **67**, 249 (1981).
37. J.W. Edington, *Interpretation of Transmission Electron Micrograph in Practical Electron Microscopy in Materials Science* (Macmillan, New York, 1975), Vol. 3.
38. M.H. Loretto, *Electron Beam Analysis of Materials* (Chapman and Hall, London, 1984).
39. R. Gervers, Phys. Status Solidi **4**, 383 (1964).
40. L.S. Shvindlerman and B.B. Straumal, Acta Metall. **33**, No. 9, 1735 (1985).
41. W.T. Read and W. Shockley, Phys. Rev. **78**, 275 (1950).
42. G. Bishop and B. Chalmers, Scripta Metall. **2**, 133 (1968).
43. H. Kokawa, T. Watanabe, and S. Karashima, Philos. Mag. (A) **44**, 1239 (1981).
44. D.H. Warrington and H. Grimmer, Philos. Mag. **30**, 461 (1974).
45. Y. Ishida and M. Mclean, Philos. Mag. **27**, 1125 (1973).
46. H. Ichinose and Y. Ishida, J. Phys. **C4**, 39 (1985).
47. H. Jang, Ph.D. Thesis, Virginia Polytechnic Institute and State University (1990).
48. *High-Temperature Ordered Intermetallic Alloys,* edited by C.C. Koch, C.T. Liu, and N.S. Stoloff (Mater. Res. Soc. Symp. Proc. **39**, Pittsburgh, PA, 1985).
49. *High-Temperature Ordered Intermetallic Alloys II,* edited by N.S. Stoloff, C.C. Koch, and C.T. Liu (Mater. Res. Soc. Symp. Proc. **81**, Pittsburgh, PA, 1987).
50. *High-Temperature Ordered Intermetallic Alloys III,* edited by C.T. Liu, A.I. Taub, N.S. Stoloff, and C.C. Koch (Mater. Res. Soc. Symp. Proc. **133**, Pittsburgh, PA, 1989).
51. *Interfacial Structure, Properties, and Design,* edited by M.H. Yoo, W.A.T. Clark, and C.L. Briant (Mater. Res. Soc. Symp. Proc. **122**, Pittsburgh, PA, 1988).
52. D. Farkas, H. Jang, M.O. Lewus, R. Versaci, and E.J. Savino, in *Interfacial Structure, Properties, and Design,* edited by M.H. Yoo, W.A.T. Clark, and C.L. Briant (Mater. Res. Soc. Symp. Proc. **122**, Pittsburgh, PA, 1988), p. 455.

53. T. Watanabe, Res Mechnica **11**, 47 (1984).
54. S. Hanada, T. Ogura, S. Watanabe, O. Izumi, and T. Masumoto, Acta Metall. **34**, No. 1, 13 (1986).
55. R. A. D. Mackenzie, M. D. Vaudin, and S. L. Sass, in *Interfacial Structure, Properties, and Design,* edited by M. H. Yoo, W. A. T. Clark, and C. L. Briant (Mater. Res. Soc. Symp. Proc. **122**, Pittsburgh, PA, 1988), p. 461.
56. D. Farkas, M. O. Lewis, and V. Rangarajan, Scripta Metall. **22**, 1195 (1988).
57. H. Lin and D. P. Pope, in *Alloy Phase Stability and Design,* edited by G. M. Stocks, D. P. Pope, and A. F. Giamei (Mater. Res. Soc. Symp. Proc. **186**, Pittsburgh, PA, 1991).
58. Th. Karakostas, G. Nouet, G. L. Bleris, S. Hagege, and P. Delavignette, Phys. Status Solidi (a) **50**, 703 (1978).
59. V. Randle and B. Ralph, Inst. Phys. Conf. Ser., No. 78, Ch. 2, 59 (1985).
60. T. Watanabe, in *Interfacial Structure, Properties, and Design,* edited by M. H. Yoo, W. A. T. Clark, and C. L. Briant (Mater. Res. Soc. Symp. Proc. **122**, Pittsburgh, PA, 1988), p. 443.
61. J. W. Wyrzykowski and M. W. Grabski, Philos. Mag. A **53**, 505 (1986).
62. V. Randle, B. Ralph, and D. Dingley, Acta Metall. **36**, 267 (1988).